ORIGINAL PAPER

Evaluating spatial patterns in precipitation trends across the Amazon basin driven by land cover and global scale forcings

Nafiseh Haghtalab[1] ⬤ · Nathan Moore[1] ⬤ · Brent Porter Heerspink[2] · David W. Hyndman[2]

Abstract

Spatial and temporal patterns of rainfall are governed by complex interactions between climate and landscape perturbations including deforestation, fire, and drought. Previous research demonstrated that rainfall in portions of the Amazon Basin has intensified, resulting in more extreme droughts and floods. The basin has global impacts on climate and hydrologic cycles; thus, it is critical to understand how precipitation patterns and intensity are changing. Due to insufficient precipitation gauges, we analyzed the variability and seasonality of rainfall over the Amazon Basin from 1982 to 2018 using high-resolution gridded precipitation products. We developed several precipitation indices and analyzed their trends using the Mann–Kendall test (Mann 1945; Kendall, 1975) to identify significant changes in rainfall patterns over time and space. Our results show landscape scale changes in the timing and intensity of rainfall events. Specifically, wet areas of the western Basin have become significantly wetter since 1982, with an increase of 182 mm of rainfall per year. In the eastern and southern regions, where deforestation is widespread, a significant drying trend is evident. Additionally, local alterations to precipitation patterns were also observed. For example, the Tocantins region has had a significant increase in the number of dry days during both wet and dry seasons, increasing by about 1 day per year. Surprisingly, changes in rainfall amount and number of dry days do not consistently align. Broadly, over this 37-year period, wet areas are trending wetter and dry areas are trending drier, while spatial anomalies show structure at the scale of hundreds of kilometers.

Keywords Rainfall seasonality · Amazon Basin · Precipitation variations · Extreme events · Precipitation indices · Climate feedbacks

1 Introduction

The Amazon basin, which contains about 60% of tropical rainforests in the world (Laurance et al. 2002; Arvor et al. 2017), plays vital roles in regulating climate patterns, sustaining ecosystem services, contributing to global biodiversity

✉ Nafiseh Haghtalab
haghtala@msu.edu

[1] Department of Geography, Environment, and Spatial Sciences, Michigan State University, 673 Auditorium Rd, Room 116, East Lansing, MI 48824, USA

[2] Department of Earth and Environmental Sciences, Michigan State University, 288 Farm Ln Bldg, Rm 207, East Lansing, MI 48824, USA

and cycling nutrients. These services, however, have been disrupted by human activities within the region due to infrastructure development and resource extraction. Deforestation is the dominant human disturbance in this region, replacing forests with pasture and agriculture across the "Arc of Deforestation" in the southern headwaters of the Amazon basin (Fearnside 2000; Costa and Pires 2010; Moore et al. 2007; Davidson et al. 2012). These land use changes have impacts across local to global scales, particularly on climate and hydrologic cycles (Longobardi et al. 2016). Land cover change affects land surface characteristics including surface albedo, roughness, and reflectance, which directly alter surface energy and water fluxes. Partitioning of these fluxes are the most important parameters in the spatial distribution and seasonal variability of rainfall. In the Amazon basin, changes in the magnitude and variability of precipitation have caused both intensified drought recurrence and flood frequency (Silva et al. 2018). Khanna et al. (2017) found that a reduction in surface roughness due to deforestation plays an important role

in the region's dry season hydroclimate, and that deforestation "is sufficiently advanced to have caused a shift from a thermally to a dynamically-driven hydroclimate regime". This loss of forest is primarily driven by agricultural expansion and infrastructure development. Walker et al. (2009) demonstrated a positive correlation between road development construction and subsequent deforestation. Simulations of the Amazon basin's hydroclimatology suggest that deforestation induced declines in rainfall across the basin's eastern and southern ecotones could lead to permanently drier conditions (Moore et al. 2007). Simulations also show that preserving forest can help maintain precipitation amounts (Walker et al. 2009). Evapotranspiration (especially transpiration) increases shallow convection, which destabilizes the atmosphere during the transition from dry to wet season. Therefore, interactions between land surface processes, atmospheric convection, and biomass burning are related to the deforestation effects on the dry season length and enhance regional vulnerability to drought (Wright et al. 2017). Soil moisture and vegetation cover type affect the net radiation through changes sensible and latent heat fluxes over the basin (Li et al. 2006), which are important factors for determining the wet season onset and the dry season length (Li and Fu 2004). This possible anthropogenic shift towards permanent savannization is not a new concept (Oyama and Nobre 2003), but evidence for the phenomenon has not been shown via broad analyses of Amazon precipitation data.

While the effects of deforestation on large scale climate patterns have been extensively studied in the Amazon basin, changes in climate extremes are also affected by synoptic-scale processes and global circulations including the El Niño-Southern Oscillation (ENSO) and the Pacific Decadal Oscillation (PDO) (J. A. Marengo and Espinoza 2016). The observed intensification of rainfall at the basin scale is most likely due to higher sea surface temperatures in the Atlantic (Gloor et al. 2013). This is consistent with an intensification of the global water cycle. Specifically, ENSO cycles that occur every 3 to 7 years can exacerbate droughts during the dry season (Laurance et al. 2002). Conversely, when equatorial Pacific and Northern tropical Atlantic are anomalously cold, a rainier wet season is commonly observed. In addition, when some oceanic events are combined, such as cold SSTs and El Niño, the northern Amazon faces strong negative rainfall anomalies (Ronchail et al. 2002). Therefore, changes in precipitation in the Amazon basin can be related to sea surface temperature fluctuations, ENSO, the Pacific Decadal Oscillation (Marengo and Espinoza 2016), and deforestation (Khanna et al. 2017). However, changes in each factor may manifest differently within the hydroclimatic cycle, and across portions of the basin.

Quantifying changes in precipitation variability is essential to analyze effects on ecosystems. To capture variability, high-resolution analysis of rainfall over the entire Amazon basin is needed. Precipitation at the regional scale is far from uniform (Laurance et al. 2002); at finer scales, it is influenced by convection resulting in enhanced spatiotemporal variability (Funatsu et al. 2012). Several trends in mean and variance have been identified throughout the Brazilian Amazon using weather stations. For example, Marengo (2004) found a negative trend in rainfall for the entire Amazon basin based on gauge measurements from 1929 to 1998, while the Mann–Kendall test used on multi-decadal station datasets found only weak trends (Satyamurty et al. 2010). Trend analysis of daily gauge precipitation data of 305 weather stations from 1983 to 2012 showed a significant positive trend in the number of days with precipitation more than 50% and 95% quantiles in the northeast region and a significant decreasing trend in the number of days with precipitation above 95% quantile in the south of the basin (Santos et al. 2015). More negative than positive precipitation trends were detected during the transition months from wet to dry (and vice versa) over deforested areas using rain gauges from 1971 to 2010; the rainy season length was reduced at 88% of the rain gauges in 1971–2010 with a later onset and earlier cessation, along with more drying conditions in the rain gauges located in deforested areas than the ones on forested locations (Debortoli et al. 2015). In contrast, Almeida et al. (2016) found no trend at most of the 47 weather stations in the Brazilian Legal Amazon from 1973 to 2013.

Remotely sensed data have been used to evaluate synoptic changes in rainfall patterns due to insufficient spatial distribution of weather stations and inconsistent temporal measurements of gauge data (Silva et al. 2018; Arvor et al. 2017). Climate extreme indices have been developed for both precipitation and temperature but show a distinct spatial pattern in significance (Da Silva et al. 2019). Salviano et al. (2016) used the Climate Research Unit (CRU) monthly precipitation data (1961–2011) and the Mann–Kendall test to estimate rainfall trends across Brazil and found an insignificant positive trend in the wet season (Jan-Apr) and an insignificant negative trend in the dry season (Jun-Sep). Analysis of PERSIANN_CDR (Precipitation Estimation from Remotely Sensed Information using Artificial Neural Networks—Climate Data Record (Ashouri et al. 2015) daily precipitation data detected significant decreasing rainfall trends associated with contracting wet season in the southern Amazon basin, which are possibly connected to human drivers (Arvor et al. 2017). Some contrary results have also been reported: Tropical Rainfall Measuring Mission satellite (TRMM) data from 1998 to 2015 were analyzed using the Mann–Kendall test to quantify precipitation trends over the Brazilian Legal Amazon at the 5% significance level. An annual pixel-by-pixel analysis showed that 92.3% of the Brazilian Amazon had no rainfall trend during the period analyzed, while 4.2% had significant negative trends ($p \leq 0.05$) and 3.5% had significant positive trends (Silva et al. 2018). Arvor et al. (2017) analyzed changes in seasonality of the Southern Amazon from 1983 to 2014 and found a

contraction of the rainy season by several days. Also, the frequency of dry days in the southern Amazon has increased significantly, and total rainfall has decreased for the same region. While wet day frequency has increased across northern Amazon along with an increase in total rainfall about 17% (Espinoza et al. 2019).

Previous publications on precipitation change in the Amazon basin provided contradictory results, perhaps due to either insufficient spatial distribution of weather stations, the low spatial resolution gridded datasets, or analysis limited to subregions of the basin. This discrepancy motivates our analysis of variability in higher spatial resolution precipitation datasets at daily timescales. Here, we analyze changes in precipitation over time and space for the entire Amazon Basin. We examine the trends and change points using CHIRPS data from 1982 to 2019 along with possible drivers such as deforestation, ENSO, and/or changes in the Southern American Convergence Zone (SACZ). We define indices (Number of Dry Days (NDD) and Number of eXtreme Events (NXE) for both wet and dry season, and Mean Annual Precipitation (MAP) per day) to analyze changes beyond wet days and dry days since the combination of these changes can provide new insights on how different processes are changing across seasons. Ultimately, the aim is to correlate significant and spatially cohesive precipitation variability to causal factors.

2 Material and methods

2.1 Study area

The Amazon basin, which spans ~6 million km^2, is drained by the Amazon River and its tributaries. It covers portions of Brazil, Colombia, Peru, Bolivia, Ecuador, Guyana, Suriname, and Venezuela and includes the Andes Cordillera where the transition between lowland and mountains results in the rainiest areas of the basin (Espinoza et al. 2015; Paccini et al. 2018) (Fig. 1). The river system is a hotspot of ecological diversity and ecosystem function; it provides more than 20% of the world's freshwater discharge, and its forest biomass holds about 100 billion tons of carbon (Malhi et al. 2006; Saatchi et al. 2007). Forest vegetation cover has decreased to 80% of its pre-1960s area (Instituto Nacional de Pesquisas Espaciais and National Institute for Space Research Projeto Prodes Monitoramento da Florsta Amazonica Brasileira por Sate'lite Prodes 2011). The rate of deforestation decreased from 28,000 km^2/year in 2004 to less than 7000 km^2/year in 2011 (Davidson et al. 2012); however, it is increasing again (Fearnside 2015). In addition to landscape changes, the population of the Brazilian Amazon increased from ~6 million in 1960 to ~25 million in 2010 (Davidson et al. 2012).

Climate varies over the region, from the continuously rainy northwest to the wet/dry transitional climate and long dry season in the south and east (Sombroek 2001; Davidson et al. 2012). The climate gradient is consistent with the land cover change gradient, with more conversion to agriculture in the dry east and south of the region referred to as the "Arc of Deforestation." The eastern basin is strongly influenced by ENSO (Marengo 2004), in which flow in the Amazon River decreases during El Niño years; correspondingly, flooding increases during La Nina years (Coe et al. 2002). The Atlantic Multi-decadal Oscillation also affects the region; for example, the severe drought of 2005 is linked to this oscillation (Marengo et al. 2008). In the southern portion of the basin, maximum rainfall occurs during DJF (the austral summer) related to the South American Monsoon System (SAMS; Vera et al. 2006), which brings moisture from the equatorial regions such as tropical Atlantic Ocean. The SACZ contributes to rainfall variability across southern Amazonia during JJA (the austral winter), which is an elongated northwest/southeast band of convection (Carvalho et al. 2004). The ITCZ highly influences MAM rainfall regime, but it is highly variable (e.g., Fu et al. 2001).

2.2 Data

2.2.1 Rain gauge data

Daily rainfall datasets from 1982 to 2018 for the Brazilian Amazon basin were acquired from a network of 424 rain gauging stations operated by the Brazilian National Water Agency (ANA). For this analysis, we excluded all stations missing greater than 5% of data per year, then subsequently excluded all stations with a record shorter than 10 years after 1982. This resulted in 198 stations over the study area, which had at least 10 years of daily data with less than 5% of daily values missing per year.

2.2.2 Remotely sensed precipitation data

We examined several gridded datasets available at different spatial and temporal resolutions for the region. TRMM 3-hourly data with 0.25° spatial resolution is available starting in 1998 (Huffman et al. 2007), but it has a relatively coarse spatial resolution and its temporal extent is insufficient for climate analysis (20 years of data). PERSIANN–CDR data contains daily precipitation estimates from 1983 to present, with 0.25° spatial resolution (Ashouri et al. 2015). This data also has coarse spatial resolution and some artifacts for several dates for the western Amazon. The Climate Hazards Group InfraRed Precipitation with Stations (CHIRPS) dataset has 0.05° spatial resolution that incorporates satellite imagery to represent sparsely gauged locations. It used smart
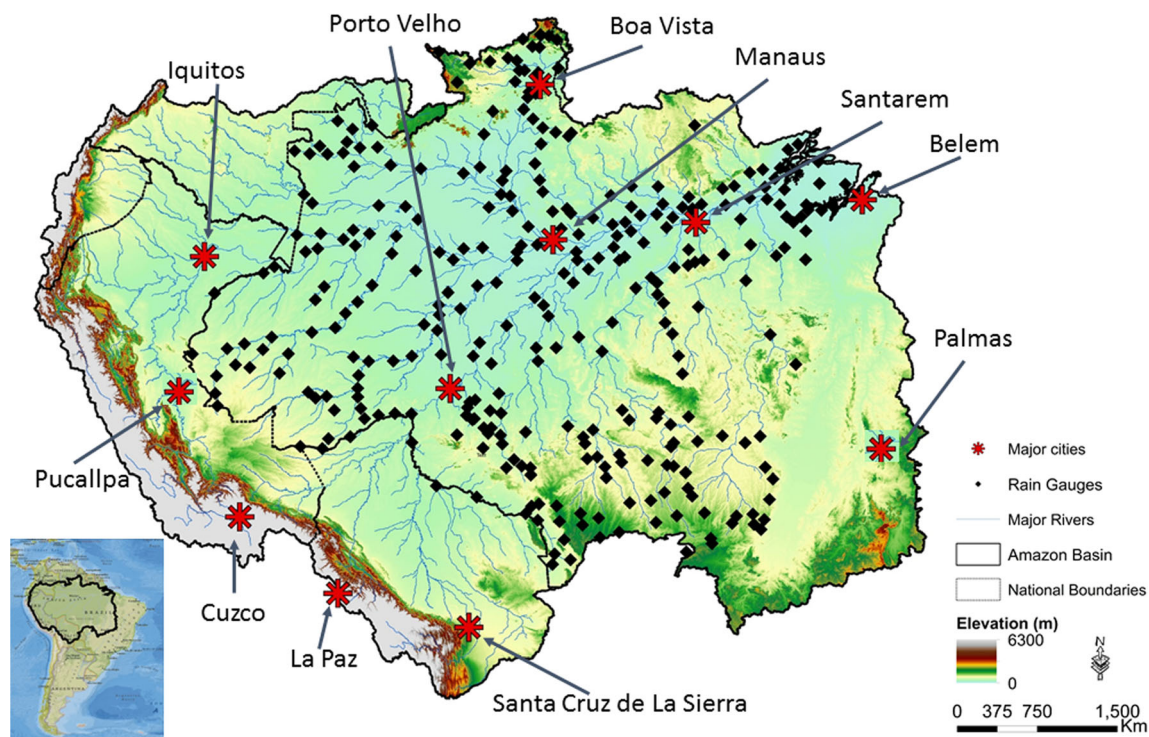
Fig. 1 Map of the Amazon basin shown with shaded topography, along with ANA gauge precipitation stations, major rivers, and cities

interpolation techniques to blend station data with remotely sensed data to provide high resolution, long period of record precipitation estimates based on infrared cold cloud duration (CCD) observations (Funk et al. 2015). CHIRPS has been checked for consistency with Global Precipitation Climatology Center (GPCC) precipitation estimates and performs better than other gridded datasets (Funk et al. 2015). More information about CHIRPS is available at chg.geog. ucsb.edu/data/chirps/. In this paper, we used CHIRPS data to analyze the trends in precipitation, and the ANA gauge data were used to verify the findings from the CHIRPS data.

2.3 Precipitation indices

We defined several indices to quantify precipitation variability including number of dry days (NDD), number of extreme events (NXE) during the dry and wet season (calculated separately), and mean annual precipitation per day (MAP) for a water year (Table 1). More information regarding the threshold for NXE and NDD are provided in supplementary materials. In the next step, we ran a pixel-based non-parametric Mann–Kendall test for each of these indices. We used both Kendall's Tau coefficient and Sen's Slope estimator to detect significant time series trends from 1982 to 2018. Third, we ran a change point detection algorithm to identify anomalies and abrupt changes in all indices for regions that show statistically significant changes. Based on the water year, we separately analyzed

data for the dry and wet seasons. Here, we define the water year as the time span starting December 1 of the previous year and ending November 30 of the current year. The dry season generally starts in early May and ends in late November of the same year. Accordingly, the wet season spans from early December through the end of April. Although dry and wet seasons are not the same for all locations in the basin, for the sake of consistency and homogeneity in the analysis, we used the terms wet and dry seasons for the mentioned time frames. Changes in seasonality of the Southern Amazon by Arvor et al. (2017) found a contraction of the rainy season by several days. Similarly, Debortoli et al. (2015) found that rainy season became shorter at 88% of rain gauges from 1971 to 2010. Also, Fu et al. (2013) projected an increase in consecutive dry days and a decrease in the consecutive wet days by the end of the twenty-first century. We thus used three separate indices to examine trends in total rainfall and extremes in rainfall for the distinct seasons in the Amazon. Table 1 summarizes these indices.

2.4 Methodology

2.4.1 Change point detection

To identify the most significant breakpoint in a large dataset, we applied binary segmentation method (Fryzlewicz 2014). Binary segmentation method is suitable for consistent

Table 1 Summary of defined indices to quantify the precipitation variability

Index	Definition
Mean annual precipitation (MAP) by day	Mean Annual Daily Precipitation (mm)
Number of dry days (NDD)	Days ≤ 2 mm total precipitation
Number of extreme events (NXE)	Days ≥ than 20 mm total precipitation
Wet season	Dec. 1 to Apr. 30
Dry season	May 1 to Nov. 30
Water year	Dec. 1 of previous year to Nov. 30 of current year

estimation of the number and location of multiple change points in data. Cost functions are used in the binary segmentation to panelize a high amount of change points in order to avoid overfitting. In a given time series $\{y_{\tau+1}, .., y_n\}$, if the distribution of $\{y_1,. .., y_\tau\}$ and $\{y_{\tau+1}, .., y_n\}$ differ at time τ with respect to at least one parameter such as mean, variance, or regression structure, then a change point will be detected (Rohrbeck 2013). For our analysis, we used the model to select the most significant breakpoint in each data series.

2.4.2 Statistical analysis of rainfall trends

MAP, NEX, and NDD of dry and wet seasons were calculated and sorted using Python version 2.7.5. Statistical analyses were done using R statistical software (version 3.3.4; R Core Team 2018). Pixel by pixel analysis identified the spatial distributions of the trends. We used two non-parametric methods to identify the strengths and magnitudes of the trends in both gridded data and gauge measurements as these data are not normally distributed, and non-parametric tests are less sensitive to outliers. The widely adopted Mann–Kendall test was used to analyze trends in climate data (e.g., Wilks 2011; Zilli et al. 2017). The non-parametric Mann–Kendall test examines the distribution of data to be independent and identical. Our null hypothesis is that there is no trend, while our hypothesis states that there is a monotonic trend in time (Mann 1945; Kendall 1995).

We calculated the test statistic Tau using the "Kendall" package in R. The range of Tau is between − 1 to + 1, with negative values showing a decreasing trend (more negative "steps") and positive values showing an increasing trend (more upward "steps"). We used a significance level of α = 0.05 in this study to identify significant trends.

To quantify the trend magnitude for the three indices, the Mann–Kendall test has been widely used with the non-parametric and robust Sen's slope estimator (e.g., Gocic and Trajkovic 2013; Partal and Kahya 2006; Sharma and Babel 2014; Xu et al. 2003). Again, the distribution may deviate

significantly from a normal/Gaussian distribution for this method. This test is not sensitive to skewness or large outliers (Kumar Sen 1968). Helpful details on equations and the procedures of Sen's slope estimator and the Mann–Kendall test are described in ElNesr et al. (2010)). Among all the remotely sensed datasets, we explored CHIRPS as it had the highest spatial and temporal resolution and showed the lowest bias and the highest agreement with the gauge data (Funk et al. 2015).

3 Results

3.1 Gridded data validation

To validate the gridded data, we compared ANA rain gauge measurements to CHIRPS data. We compared all 198 ANA gauges that have more than 10 years of data after 1982 with the corresponded CHIRPS pixel values at the same location. For this analysis, the spatial average of 9 neighbors around each point was calculated to reduce bias and errors in the comparison. Figure 2 shows the spatial distribution of mean daily annual precipitation out of CHIRPS (1982–2018) and ANA stations for comparison. The significant correlations at 5% are marked by stars and at 10% are marked with double circles on Fig. 2. The results demonstrate that the northwestern portion of the Amazon basin is the wettest, and the south and southeast portions are the driest. Most of the basin receives 3 to 9 mm/day with a maximum of ~12 mm/d.

We evaluated correlations between both PERSIANN_CDR and CHIRPS against ANA gauge data.

Correlation between ANA and CHIRPS was more than 0.6 at 12% of the sites, but correlation between PERSIAN and ANA are mostly around 0.2, and there are no correlations above 0.6 (Fig. 2, bottom inset). This is not surprising as some gauge stations are used in the development of the CHIRPS product. We also encountered numerous artifacts, non-physical patterns, and missing values in the PERSIANN-CDR data. Due to this and bias corrections based on gauge data, we opted to conduct our full analysis with CHIRPS data.

3.2 Interannual precipitation trend analysis

The Tau statistic of the Mann–Kendall test is used to assess significant non-parametric trends in time series. Section 3.2 reports the Tau statistic results and Sect. 3.3 reports the Sen's slope results for the CHIRPS precipitation data.

3.2.1 MAP trend analysis

Figure 3 shows the Tau values for gridded data and gauge measurements. Only gauges with statistically significant trends are shown on the map. Forty one of the 54 gauges with trends (circles) are spatially consistent with CHIRPS

Fig. 2 **a** Annual average precipitation using CHIRPS daily values 1982–2018. Circles on the map show the correlations between CHIRPS and ANA gauges. Size of the circle indicates the strength of correlation and stars indicate the significant correlations at 5%. **b** Distribution of daily rainfall across categories based on CHIRPS daily values 1982–2018. **c** Correlation between daily rain gauges (ANA) and daily CHIRPS data in black and rain gauges and PERSIANN in orange. A table of correlation values for each of these gauges is included in Supplemental Materials
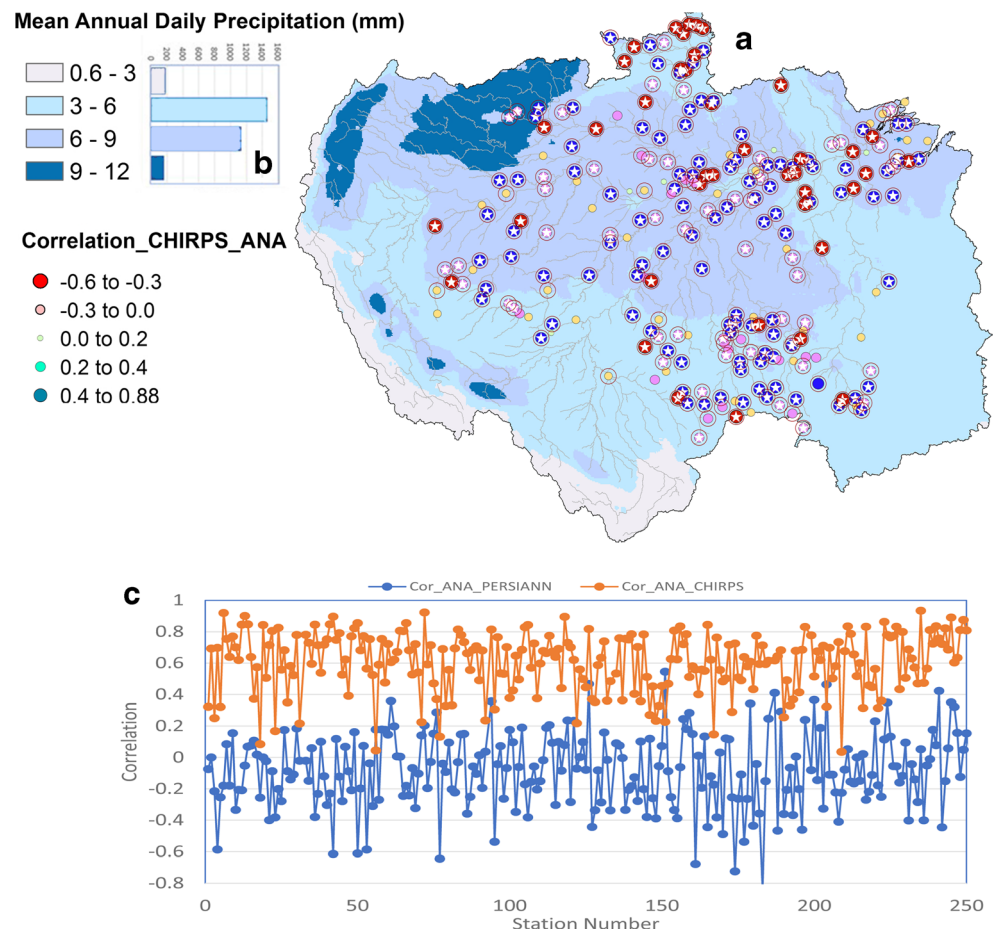
(background colors); hatched areas indicate significance at the 0.05 level. The western and northern parts of the domain show significant increasing trends with Tau > 0.3 while "hot spots" around Porto Velho and Santa Cruz de la Sierra show significant decreasing trends with Tau < 0.3.

To capture abrupt changes in time series, we chose areas with significant change to look at local precipitation variability. All significant CHIRPS pixels in each lettered sub-region on the following figures were spatially averaged for this test. The lettered regions were selected based on the outlined significance levels. Regions A (north central basin), B (central basin), and C (south central basin) of Fig. 3 show Tau values < − 0.3, indicating that there are year-to-year decreases 30% more often than the rest of the time series. Regions A, B, and C show a decreasing trends with significant variability. Also, the extreme difference between the amount of rainfall in 2013 and 2015 is considerable. Change point detection shows abrupt decreases in daily precipitation across regions A, B, and C after 1998, 1995, and 1992, respectively, which all are severe drought years across the basin, especially in the northeast. These are all ENSO years, which combined with anomalous heating in the Atlantic Ocean can cause less rainfall across the basin. Region D shows a positive Tau value of > 0.3 indicating increasing trend in MAP, with an abrupt increase after 1999; several other regions

have similar positive trends across the basin. Together, these results suggest a significant shift in mean annual precipitation across all four regions during the 1990's.

3.2.2 NDD trend analysis

Figure 4 shows the trends in NDD for the wet and dry seasons. All selected regions show an increasing trend of NDD. During the dry season, NDD increased significantly over the "arc of deforestation" in the southern and eastern portions of the basin. Increasing NDD during dry season around Santa Cruz (region E on Fig. 4) shows a graduate rise across the study period, with a sharp rise in 2010, which was an extreme El Niño year and extreme drought across the basin. 2010 was characterized by a weak SACZ, positive anomalies in the SST in central Pacific Ocean, and negative anomalies in SST in Southern Tropical Atlantic Ocean, and a displacement of the ITCZ to the north (Coelho et al. 2013). In region F, which covers a large area east of Palmas, the abrupt change point in NDD occurred in 2004 proceeding an increasing trend in number of dry days. There are two extreme decreases in NDD in 1989 and 2008, both reaching a historic low 157 dry days, while the average number of dry days during the dry season is approximately 170 days for region F.
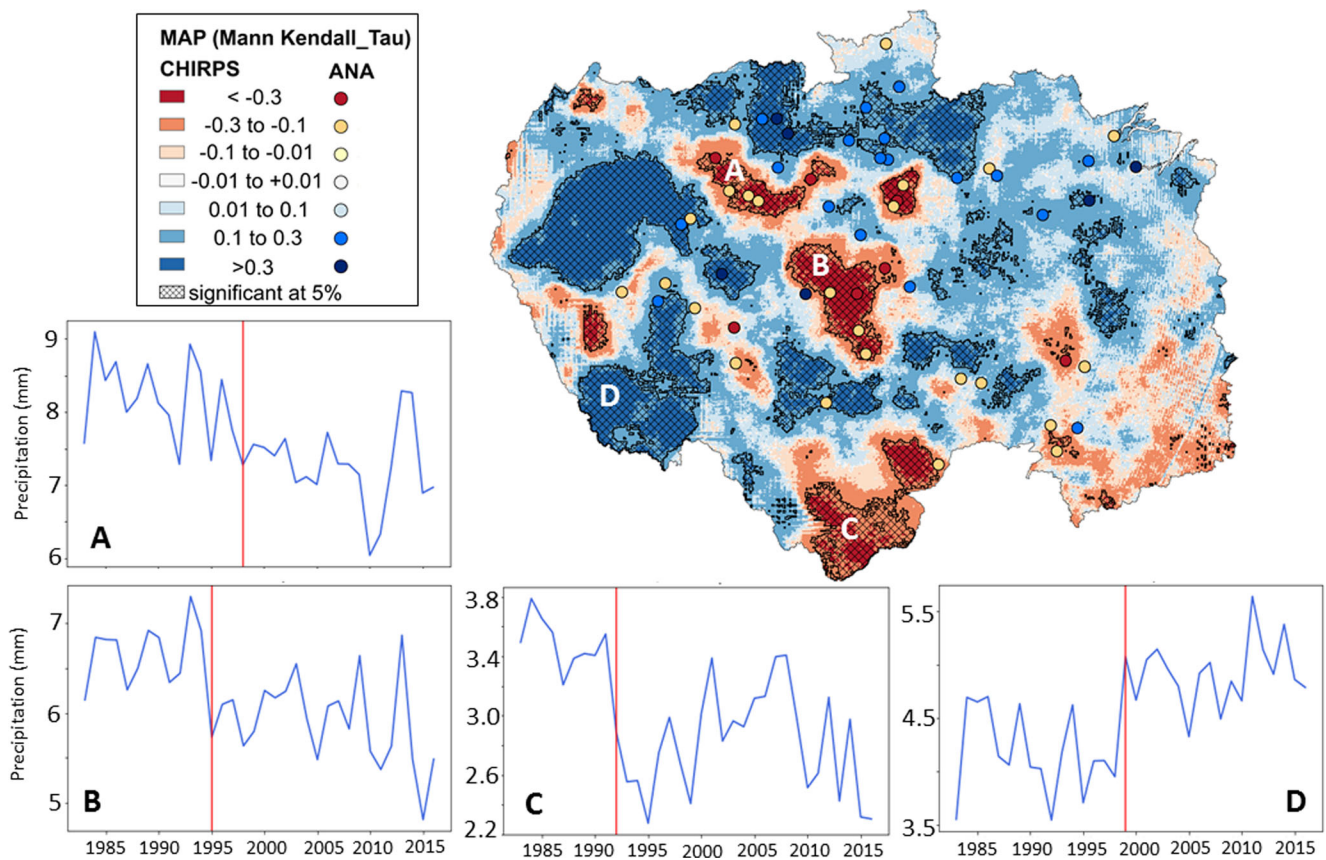
Fig. 3 Trend of mean annual precipitation (MAP) by day is shown on the map. Hatches show significant trends at 5% confidence level. Graphs show the abrupt changes in the amount of mean annual daily precipitation for the outlined significance levels. Red lines indicate significant change points. Note that vertical axis scales are different

In the wet season, changes in NDD are spatially heterogeneous based on our analysis of station data and prior research (c.f., Fig. 4 in Silva et al. 2018). While there are few significant changes at $\alpha = 0.05$ level, some changes are significant at $\alpha = 0.1$ across broad areas (not shown). Only one location shows a significant increasing/drying trend (region G). The time series for G shows high variability for this very rainy region, but the overall increasing trend is clearly recognizable. For example, NDD in 1982 was 65 days, while by 2017, it had shifted to 84 days—an increase of 20 days around Pucallpa, Peru. There was also a steep decline in NDD in 1988, to only 54 dry days within the wet season. Change point analysis identified 2001 as a significant break after which the average NDD remains consistently higher than before 2001. There is a notable inconsistency between gauge and gridded statistics for number of dry days during the wet season in the Northern Basin.

3.2.3 NXE trend analysis

Changes in NXE during the dry and wet seasons are shown in Fig. 5. Regions H, which is located on the western part of the basin, shows an increasing trend of NXE during both dry and wet season. But all other regions show a decreasing trend in NXE in both dry and wet season. In the next section, magnitude of the trends is explained comprehensively. The warmer (red) colors indicate a decrease in NXE, while cooler (blue) colors show an increase in NXE. Similar to MAP trends, NXE for the dry season shows a significant increasing trend in the west, especially around Iquitos. There is a strip in the center of the basin from north to south that shows a decreasing trend in extreme events. Gridded and station data show high consistency for the NEX metric across the domain.

Region H shows that the NXE during the dry season doubled after 2012 relative to earlier average of 11 extreme events. Based on change point detection, the abrupt increasing trend in NXE happened after 2011. Region J (around Porto Velho extending in a northwest strip) shows a large decreasing trend in NXE, with one dramatic rise in extreme events in 1989. Change point detection identifies a significant shift in NXE in 1997, which was an extreme drought year. Before this point, NEX generally remained above 8 days per year, and afterward falls and has a maximum of 7 days per year. Conversely, in the Santa Cruz de la Sierra (Region K), a noticeable and consistent drop in NXE variability occurs after 1988 (also, a severe drought year). Significant breakpoints in
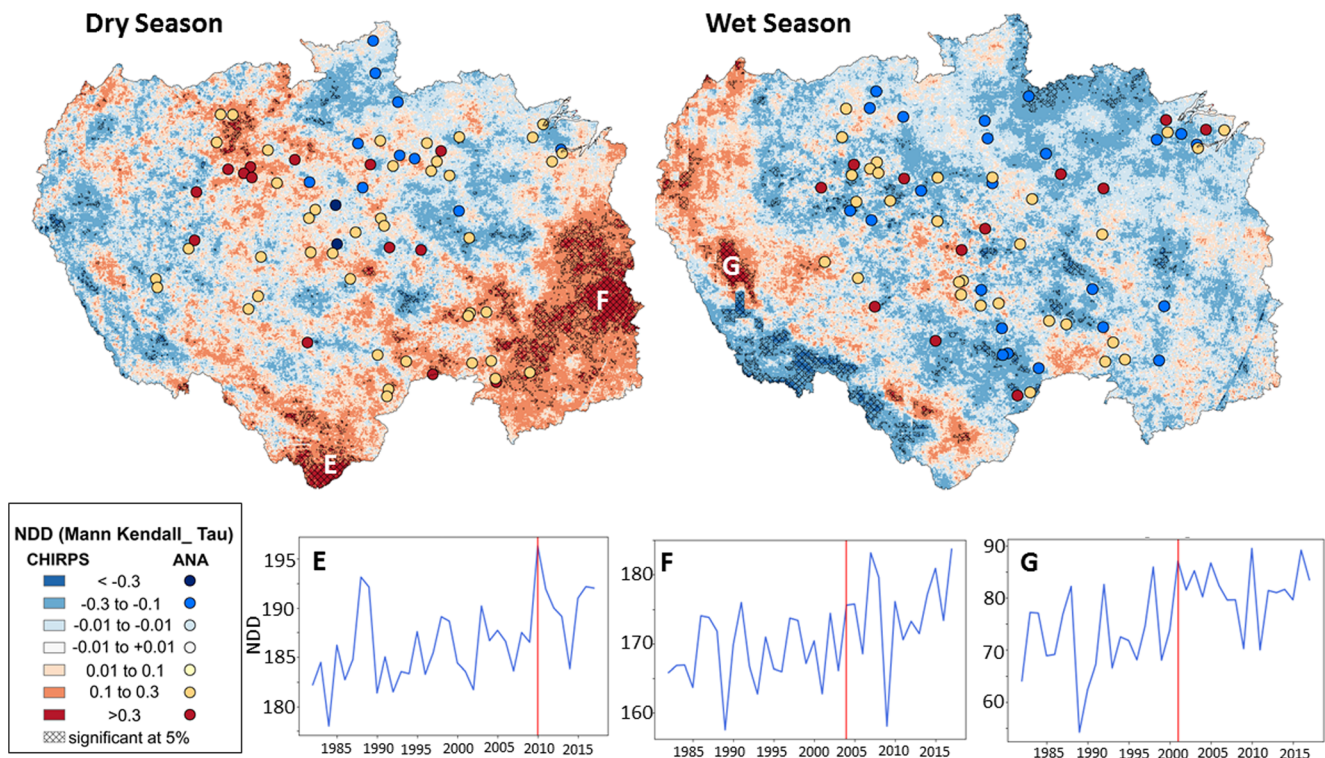
Fig. 4 Trend of number of dry days (NDD) during the wet and dry season using CHIRPS as a gridded data and ANA rain gauge measurements to validate the results. Graphs on the bottom show the NDD anomalies for each season. Note that vertical axis scales are different

the patterns of dry season NXE vary temporally across these three regions.

The wet season shows more complex patterns of change and different regions of statistical significance. Similar to NDD, there is a slight inconsistency between gauges and gridded data in the north of the region, where fewer gauges are available and reporting is less consistent. Changes in NXE during the wet season are not as strongly clustered or as intense as for the dry season.

Region L in the western basin shows a slightly increasing trend with an average of 13 extreme days per year until the change point in 2012, after which NXE rises to a maximum of 23 events per year. Regions M and N, around Porto Velho and Santa Cruz, show a decreasing trend in NXE. In Porto Velho area (M), NXE changed from 26 days in 1982 to 22 days in 2017 with change point analysis showing a significant shift trend in 1995. Region N exhibits a complex but decreasing trend that is significant but not very abrupt. There is a peak in 1988 where NXE is equal to 21 days, with a clear decline after 1992 when a severe basin-wide drought occurred.

It is worth mentioning that the breakpoints for NXE in both seasons occur at nearly the same time for region H/L and J/M.

3.3 Quantifying the trend magnitude

Sen's slope is a common non-parametric method that has been used to quantify the magnitude of slope (changes per unit of time) as opposed to the "step"-counting of the Tau statistic. In this section, we discuss the magnitude of trends for each variable. Figures 6, 7, and 8 show both a standard regression line and Sen's non-parametric slope, as well as outliers and intervals. Categories and color schemes are consistent on Figs. 6, 7, and 8 to facilitate comparison between the three indices. For changes of magnitude in individual years, please see Figs. 3, 4, and 5.

3.3.1 MAP trend magnitude

Figure 6 shows Sen's slopes of the trend line for MAP. Most of the basin show statistically significant increasing trends (blue) broken up by clusters of negative trends along the Porto Velho-northwest strip. Region O (see inset graph in Fig. 6, averaged over the significant area) shows an almost sinusoidal changes with a gradual decline. This trend differs from region P near Porto Velho, which suggests a different physical process. For region O, MAP decreased by ∼ 0.2 mm/year on average over 37 years. The confidence intervals of the trend line show several outliers in the dataset that each have a different influence on the trend magnitude. 1983 was an extreme wet year for this area at a MAP rate of 9.1 mm/day. 2010 and 2011 were extreme dry years with 6 mm/day.

In region P around Porto Velho, MAP decreases annually at a rate of 0.3 mm/day. Sen's slope is approximately the same as at region O, and the overall change for 37 years is 10 mm/day
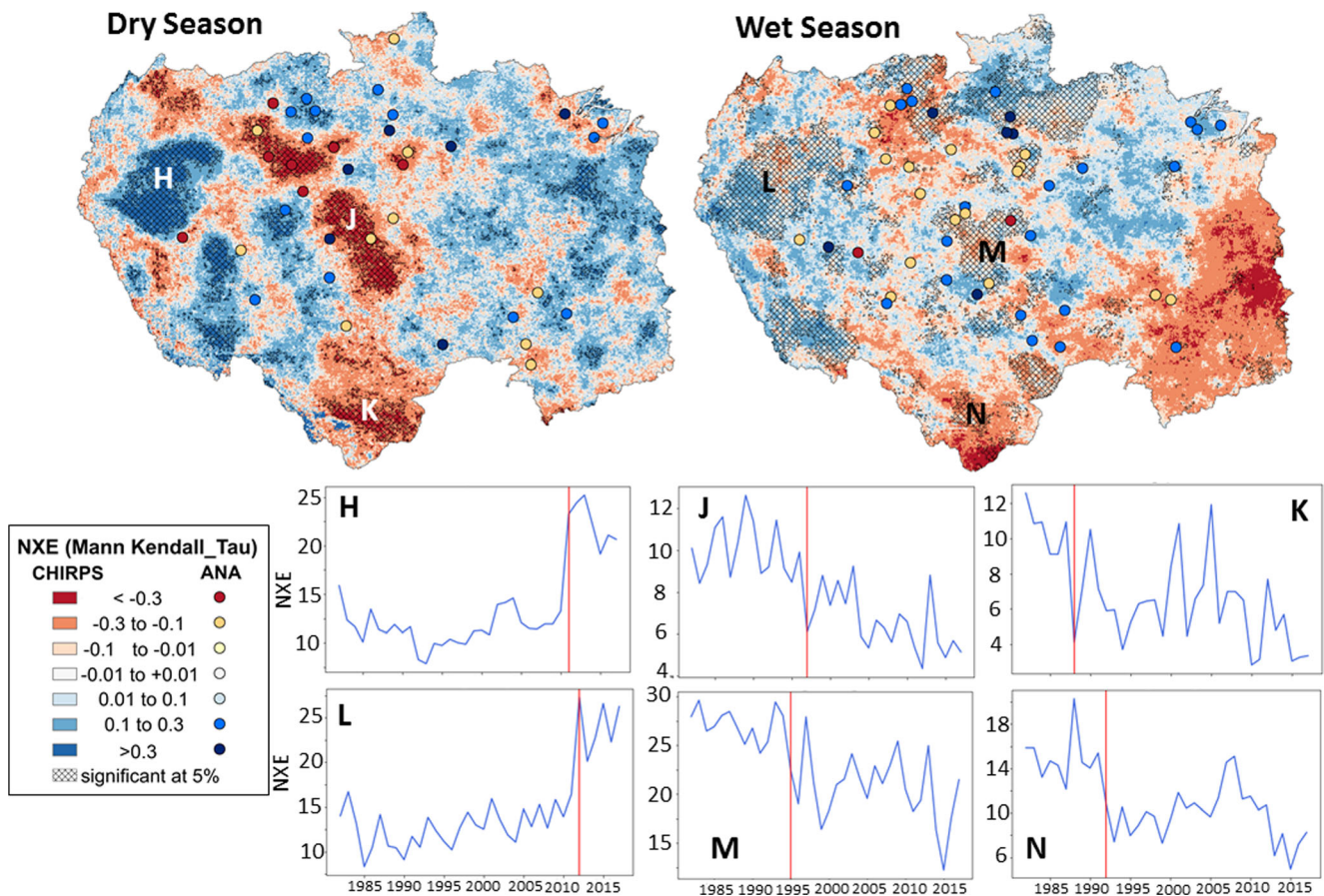
Fig. 5 Trend of number of extreme events (NXE) during the wet and dry season using CHIRPS as a gridded data and ANA as rain gauge measurements to validate the results. Graphs 5H to 5N show the NXE change points for each season with letters corresponding to regions on the map. Note that vertical axis scales are different

less in this very wet region. In 1993, an extreme wet year, region O had a MAP rate of 7.4 mm/day, and at the dry extreme (2015), a rate of 4.6 mm/day. This region barely registered the drought of 2005. However, the effects of the drought of 2015 are clear in regions O and P.

Region T, around Santa Cruz, saw a decrease of ~11 mm/year in MAP over 37 years, equivalent to 407 mm since 1982. This contiguous area of significant change spans ~ 172,000 km^2. There was a period of low variability prior to 2000, while in 2008 and 2009, and there was a sharp decline to 2.2 mm/day after 2016. Region R around and north of Cuzco shows a significant increasing and spatially cohesive trend with a magnitude of 10.1 mm/day over all the study period. 1982, 1992, and 1995 are identified as the driest years with 3.6, 3.5, and 3.7 mm/day of precipitation, whereas 2012 is the wettest year with 5.6 mm/day of rain.

3.3.2 NDD trend magnitude

Sen's slope analysis for NDD shows similar areas of significant change as the Tau method; however, magnitudes of change differ. Figure 7 shows changes of NDD across

the basin assessed using Sen's slope, which for region S indicates that the NDD of dry days during the dry season increased by about 0.3 days per year, or 11 days total over the last 37 years. Extreme values in the dataset affect the slope significantly for region S. The lowest NDD was 1984 with 176 dry days within the dry season, and 1988 and 2011 had the driest dry season with 193 and 197 dry days per season accordingly.

Across region U, NDD increased by 0.5 days per dry season or 18 days over the entire period. 1989 and 2009 had the wettest dry seasons with 156 dry days, and 2007 and 2017 had the longest dry seasons with ~ 183 dry days. NDD fluctuations in this region occur in 10-year cycles, indicating a strong influence by the Pacific Decadal Oscillation.

Region V is the only statistically significant area that showed a significant increasing trend in NDD for the wet season at the 0.05 level. NDD increased by more than 18 days over 37 years shifting from 54 days in 1989 to 89 days in 2016. This region is on the wet western edge of the basin, but the drying trend is spatially consistent with extreme increases in oil palm cultivation and fire expansion (Gutiérrez-Vélez et al. 2011).
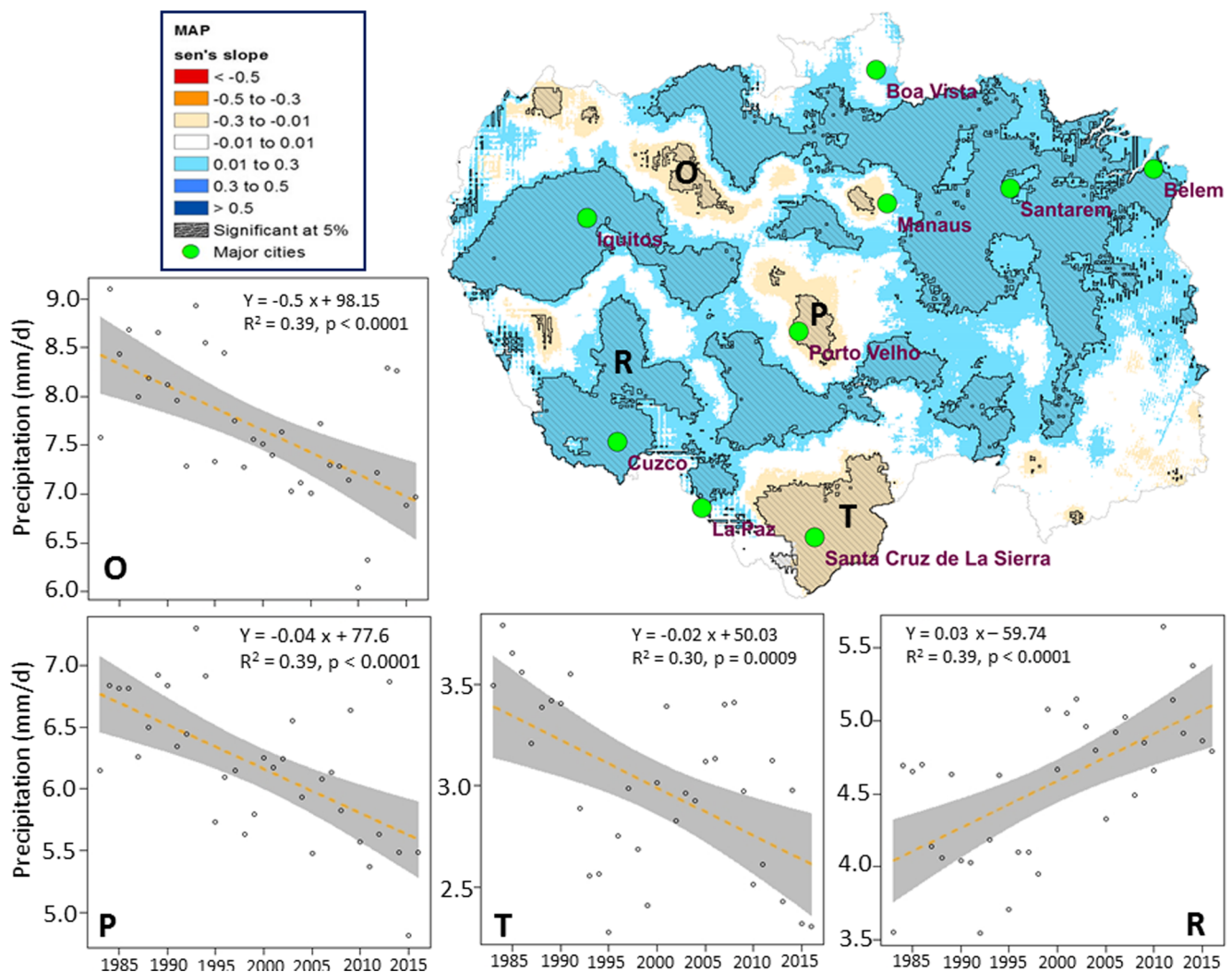
Fig. 6 Magnitude of changes in mean annual precipitation (MAP). Hatches on the map show the significant changes at 5%. Graphs show the trend line and associated equation for the significant changes with 5% confidence intervals around the trend

3.3.3 NXE trend magnitude

The Sen's slope estimators are shown spatially in Fig. 8, with selected time series in the inset boxes. Changes in NXE during the dry season shows a similar pattern with those of MAP, which indicates the intensification of the hydrologic cycle. NXE during dry season showed a large increase over most of the western region. We will use the term "events" for days that had an extreme event.

For region W during the dry season, magnitude of changes for much of the area was + 0.5 events/year, which amounts to an additional 18 extreme events on average over 37 years during the dry season. These significant changes that are tightly clustered in the last 7 years show a strong and significant increasing trend with a maximum of 26 days during the dry season of 2013.

Regions X and Y show a significant decreasing trend with 10.8 days on average over the study period, but the distribution of extreme events over time is very different. For region

X, range of NXE spans from 1989 with 13 extreme days to 2011 with 5 days—is the lowest over the 37 years. But, in region Y, NXE shows a prominent decline after 1990. The maximum NXE occurred in 1982 with 13 events, while after 2010, there were consistently less than four extreme days except for a jump in 2012 to 8 days. The minimum NXE was in 2010 at 2 extreme events.

During the wet season, region Z (Fig. 8, inset) shows an increasing trend, echoing the dry season in trend and location near Iquitos. The largest number of extreme rainfall events was in 2012, at 29 events; the following years were all well above normal and influenced the entire time series, which increased the slope of the trend line dramatically. The NXE change amount added 18 event-days on average for the study period. 1985 had the fewest NXE at about 7 days, while 2012 had 29 for the season. The data show a strong discontinuity starting around 2012, before which no year had more than 20 events during the dry season.
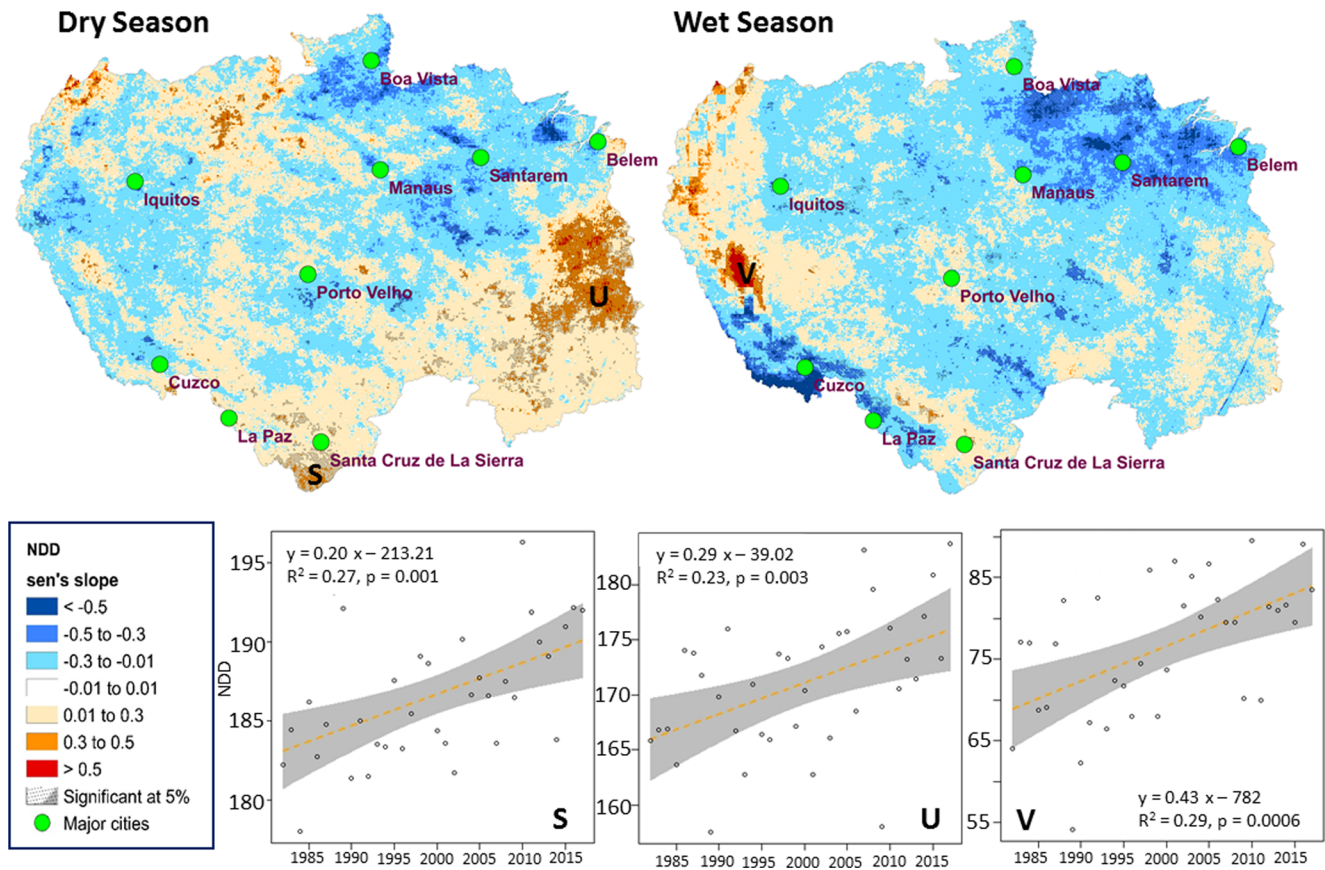
Fig. 7 Magnitude of changes in number of dry days (NDD) for the dry and wet season. Hatches on the map show areas with significant changes at 5%. Graphs show trend lines for significant changes with 5% confidence intervals around the trend. Note that vertical axis scales are different

Zones AZ and BZ both have a nonlinear interannual pattern with a local minimum in the late 1990s. NXE decreased by more than 18 events in AZ and 11 events in BZ over all 37 years during the wet season. NXE across AZ changed from a maximum of 30 events in 1983 and 1993 to a minimum of 11 events in 2015. While in BZ the maximum NXE was 20 in 1988, and the minimum NXE within the wet season was 5 events/year in 2015 (Fig. 8).

3.4 Aggregated change analysis

Figure 9 shows deforested areas in yellow from 1992 to 2015, overlain with areas of significant change in all indices to identify the extent to which deforested regions are aligned with the areas of significant precipitation changes. Areas around Porto Velho and Santa Cruz show the highest amount of deforestation and the largest extent and greatest magnitude of dryness. All indices show less precipitation for these regions. Loss of tropical rain forests is expected to have the largest landscape conversion related effect on precipitation. The yellow shaded areas on the map represent the loss of forest land, but do not capture the conversion of the native Cerrado in the far eastern side of the basin. The most significant deforestation occurred from 1994 to 2005. These heavily deforested areas (Fig. 9) are

spatially aligned with the regions with the highest precipitation variability, according to Fig. 4.

4 Discussion

The Amazon basin continues to have a rainy northwestern region, a wet/dry cyclical climate in the center of the domain, and a long dry season in the south and east (Davidson et al. 2012). Due to the Andes Mountains on the western edge of the basin, moisture cannot easily escape; our analysis finds no change in the precipitation behavior of this portion of the domain. Moisture flux from the Atlantic continues to drive the overall seasonality and transport of rainfall. However, these results show that the spatiotemporal variability of rainfall from 1982 to 2018 across the Amazon basin is locally more complex than the common refrain "wet gets wetter and dry gets drier" (Donat et al. 2016). This is verified at the extreme western and southeastern parts of the domain. We find two broad patterns of change: a synoptic-scale shift of more dry days to the south and east and spatially cohesive regions with drying and wetting trends over hundreds of km². This study does not investigate causality; determining drivers of rainfall change would require process-based
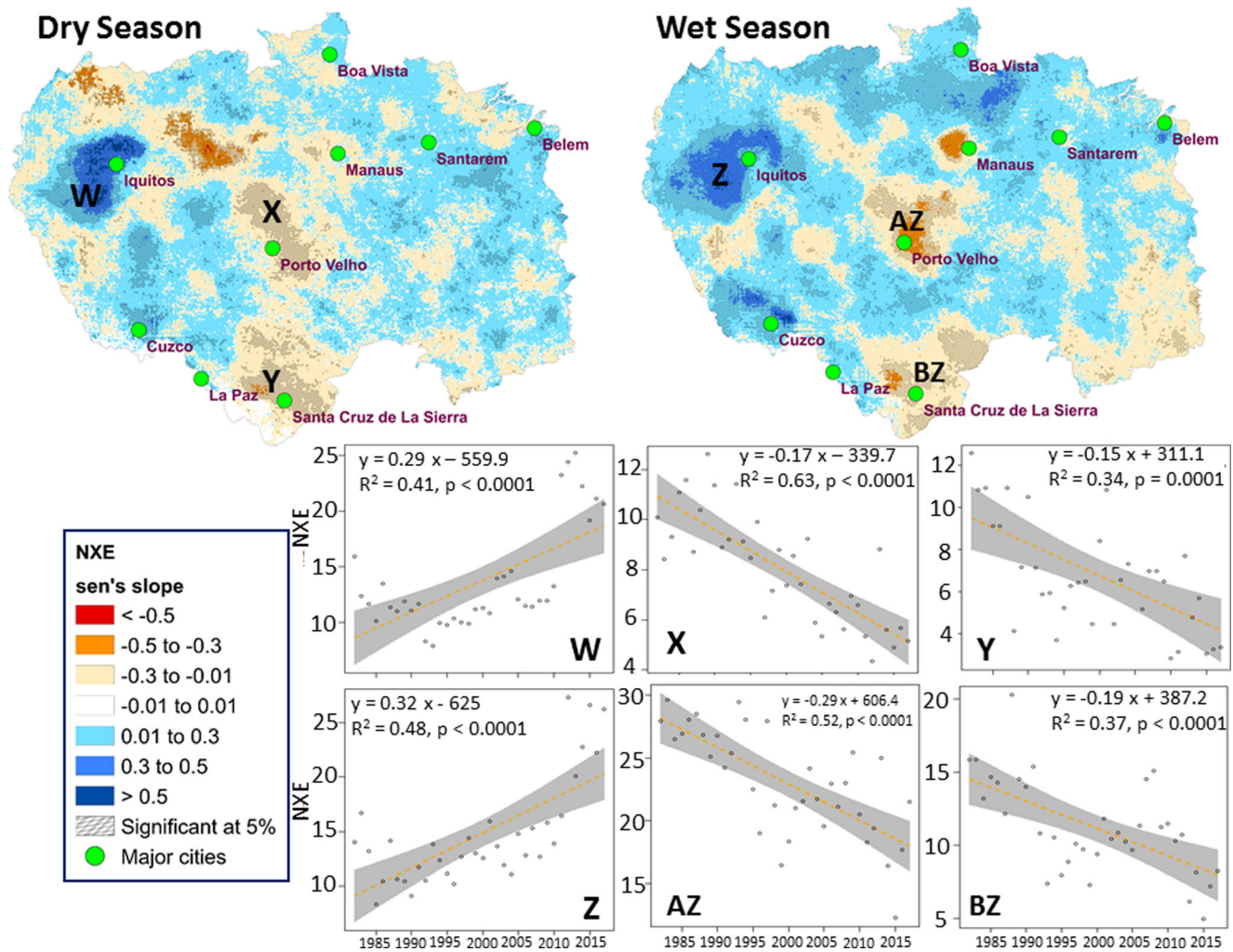
Fig. 8 Magnitude of changes in NXE for the dry and wet season. Hatches on the map show areas with significant changes at 5%. Graphs show the trend line and associated equation for the significant changes with 5% confidence intervals around the trend. Note that vertical axis scales are different

Fig. 9 Deforested areas from 1992 to 2015 are shown in yellow. Significant changes in all indices are plotted on top to show the spatial agreement between deforestation and precipitation changes. The warmer colors in the legend indicate regions with drying trends and cool (blue) colors show regions with increasing precipitation (NXE: number of extreme events; NDD: number of dry days; MAP: mean annual precipitation by day)
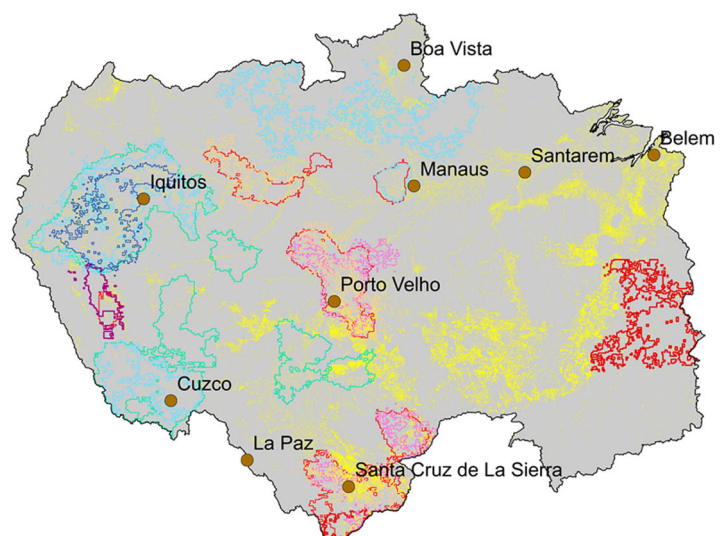
regional climate models. Instead, we refer to patterns found from this work that have been causally linked by other literature. We then consider possible drivers of precipitation change to motivate further investigation of causal mechanisms.

In our analysis, we found five important characteristics of changing rainfall patterns. First, estimates of spatial changes in MAP align with those in NXE based on both the Tau statistic and Sen's slope. This indicates that increasing frequencies of heavy rainfall days are strongly related to increases in total annual rainfall, while decreasing heavy rainfall days decrease total annual rainfall. This change shows that the distribution of rainfall has changed to more intense rainfall in some areas and reduced intensity in others. Haylock et al. (2006) reported similar results for extreme events across South America, noting that "the pattern of extreme events was generally the same as that for total annual rainfall". NDD is notably different than NXE and MAP, indicating broadly a different set of climatic processes driving these changes. For eastern Brazil, the "wet gets wetter, dry gets drier" mnemonic holds for NDD. The change point analysis showed that mean MAP changed abruptly in 1990s for all regions, NDD trend changed in 2000s, and NXE of western wet of the basin changed 2010s (regions H and L, Fig. 5). NXE of regions around Porto Velho (regions J and M, Fig. 5) hanged abruptly nearly at the same time in both dry and wet season in 1990s. But it is very varied for Santa Cruz.

Second, changes in land use—particularly shifts in deforested areas—are spatially associated with regions of modified rainfall. Figure 9 illustrates this similarity, with deforested areas near many of the regions of changed precipitation analyzed here. Higher precipitation events have been connected to the "vegetation breeze" in the Amazon (Laurance et al. 2018; Nobre et al. 2016; Sheil and Murdiyarso 2009). In such cases, large convective circulations can develop from differential heating, and be advected downwind such that the landscape change generating the convection does not receive the rainfall. This essentially rearranges rainfall into a wet/dry "dipole" associated with forest removal and road development (Moore et al. 2007; Saad et al. 2010). Thus, the extreme events may still be generated by landscape heterogeneities, but those extreme events are often advected elsewhere; for example, extreme events have declined in both the Porto Velho and Santa Cruz regions in both wet and dry seasons with MAP increases nearby. However, the main deforestation wave occurred primarily from 1992 to 2015. Since our study looked at trends during 1982–2018, this indicates other factors are likely at play, including effects associated with elevated greenhouse gases.

Third, these basin-wide results are consistent with previous rainfall studies that identified similar spatial anomalies (e.g., Ronchail et al. 2002; Silva et al. 2018) and declines in the number of extreme events in the south of the basin (e.g., Santos et al. 2015). General circulation model (GCM) outputs show highly varied historical changes over the Amazon but are not entirely consistent. IPCC AR5 results do not have sufficient resolution to characterize such changes in precipitation. Several regional climate projections at finer resolutions match some of the features found here, such as Fig. 4.4 in (Marengo and Espinoza 2016) for the 2011–2040 period. However, five of the 11 models in Ronchail et al. (2002) and Li et al. (2006) predicted an increase in annual rainfall, while three others showed a decrease and the remainder produced no significant changes in the rainfall amount for the entire basin. Wet season NXE (Fig. 5) somewhat matches maps showing fire risk by 2050 (Fig. 4 in Davidson et al. 2012), but projections are equivocal at best in matching overall historical patterns. Attribution of these changes is often difficult and requires finer-scale simulations forced with historical boundary conditions to assess causality.

Fourth, a "diagonal pattern" of decreased rainfall from the Porto Velho region to the northwestern edge of the domain appears in both NXE and MAP but is not associated with deforested regions or other major surface cover changes. A similar diagonal structure is evident in Silva et al. (2018) albeit with lower statistical significance using TRMM through 2015. The wet/dry "dipole" pattern noted above may amplify this pattern. The reduction is stronger in the dry season when prevailing winds are from the south. This bimodal pattern is not produced in studies exploring land cover change alone (Bagley et al. 2014; Wu et al. 2017). However, the drying diagonal pattern shows spatial similarity with rainfall correlations to South Atlantic SST (Yoon and Zeng 2010). The South American low level jet and the South American Convergence Zone that affects rainfall in the western part of the basin are currently exhibiting higher variability (Liebmann et al. 2004). Grimm and Zilli (2009) showed that changes in precipitation variability are likely connected to ENSO and other global phenomena such as SST anomalies in the southern tropical Atlantic. Across the equatorial Amazon, Atlantic SST is strongly correlated with the timing of rainy season onset and end, especially during the transition between wet and dry regimes (Liebmann and Marengo 2001).

Fifth, a pattern of less precipitation in the south, consistent with reduced rainfall recycling (Eltahir and Bras 1994), makes seasonal changes more broadly consistent with an intensifying Hadley circulation. The weakening of poleward expansion of Hadley cells over South America has significant effects on precipitation anomalies (Freitas and Ambrizzi 2015) and has thus increased the dryness over the region, especially in northeastern Brazil (Lau and Kim 2015). Stronger Hadley and Walker circulations are associated with a lengthening dry season in South America (Agudelo et al. 2018). That moisture is moved to the interior; wetting trends in much of the Amazon basin are influenced by a strengthening Walker circulation (Barichivich et al. 2018), which we identified in the northern and western parts of the basin (Fig. 3). Yin et al. (2014) reported competing causes of variability in wet season onset that

include SSTs and more local factors. The patterns we find for both NDD and NXE affirm this picture of multiple competing drivers.

Some significant changes in specific locations are worth noting. In the western basin, around Iquitos, MAP has increased by 10.8 mm/day over the 37 years with a clear trend, with erratic behavior in dry season extreme events. Most of the increase occurred due to wet season extreme events (18 additional events over 37 years). There is significant deforestation in this region due to increased economic activity, including for palm oil cultivation. The region around Porto Velho has declined in both MAP and NXE, and a smaller decline in NDD is evident. This is similar to the pattern identified in Silva et al. (2018) using TRMM data, and the wet/dry pattern matches significant agricultural expansion in Rondonia along highway BR-364. The region around Santa Cruz has seen both significant deforestation similar to Porto Velho, but also experiences the broader southern drying trend connected to global circulations. The Eastern Basin has witnessed the most dramatic shrinking of rainy days, with NDD during the dry season increasing by more than 18 days over the study period. This drying pattern in the east, spanning the cerrado-moist forest ecotone, is likely related to agricultural expansion. Spera et al. (2016)) showed that when cerrado vegetation is replaced by agriculture, rainfall declines of up to 3% are possible.

The wet get wetter, dry gets drier perspective is only true for some regions. The dry season has lengthened in most of the eastern and northern regions of the basin to 9 months (Li et al. 2006). And, in the Iquitos region, topographic moisture convergence forced against the eastern slope of the Andes by easterly trade winds from the Atlantic causes a shorter dry season and wetter wet season (Kleeman 1989). However, correlations to other drivers make the results more complex. For example, the Eastern region is highly influenced by ENSO (Coe et al. 2009; Marengo 2004). The long dry season here is also driven by subsidence connected to both ITCZ (Fu et al. 2001) and SSTs (Yoon and Zeng 2010). Looking broadly at specific variables, dry season length is highly influenced by both the SST of tropical oceans (Liebmann and Marengo 2001) and local soil moisture and vegetation cover (Nepstad et al. 2008; Li and Fu 2004). Ronchail et al. (2002) found that the colder northern tropical Atlantic and equatorial Pacific makes the northern part of the basin wetter, as Tropical SST significantly influences this region. The shorter and drier wet season is associated with El Niño events.

5 Conclusion

Precipitation is changing in multiple ways across the Amazon basin. Here, we show that most of the Amazon basin has experienced climatic changes, many of which are significant. Generally, while the western regions have trended wetter, the eastern and southern regions trended dryer. Wetting trends occur following the spatial pattern of extreme rainfall events, with very little similarity to changes in the number of dry days. We found statistically significant changes of precipitation from 1982 to 2018 at the 0.05 level for MAP across much of the domain. Our results broadly echo those of Silva et al. (2018) but over a longer time period and with additional variables. Their constraint of a 0.05 significance level was more rigorous but may have excluded noisier but important trends.

To the best of our knowledge, this is the first study to consider the analysis of dry day occurrence and extreme rainfall event frequency during dry and wet seasons for entire Amazon basin using high temporal and spatial resolution data. The spatial pattern drivers of climate and its variability are complicated over the basin. The patterns we identified are likely a combination of factors including ENSO, SSTs, the ITCZ/SACZ transition, strengthening Hadley and Walker circulations, and deforestation. Future research should be directed towards identifying causality for these processes using high-resolution regional models. Our next steps are to simulate the effects of deforestation with and without elevated greenhouse gases to map where each process dominates and to quantify the magnitude of each perturbation. Ultimately, these simulations along with the analysis presented above will be crucial to understand changes in stream flow and hydrology, including those in flood and drought frequency across the basin.

Compliance with ethical standards

Conflict of interest   The authors declare that they have no conflict of interest.

References

Agudelo J, Arias PA, Vieira SC, Martínez JA (2018) Influence of longer dry seasons in the southern Amazon on patterns of water vapor transport over northern South America and the Caribbean. Clim Dyn 52(5):1–19. https://doi.org/10.1007/s00382-018-4285-1

Almeida TDC, Oliveira-Júnior JF, Cubo P (2016) Spatiotemporal rainfall and temperature trends throughout the Brazilian legal Amazon, 1973-2013: rainfall and temperature trends throughout the Brazilian legal Amazon. Artic Int J Climatol. https://doi.org/10.1002/joc.4831

Arvor D, Funatsu BM, Michot V, Dubreui V (2017) Monitoring rainfall patterns in the southern amazon with PERSIANN-CDR data: long-term characteristics and trends. Remote Sens 9(9). https://doi.org/10.3390/rs9090889

Ashouri H, Hsu K-L, Sorooshian S, Braithwaite DK, Knapp KR, Cecil LD et al (2015) PERSIANN-CDR: daily precipitation climate data record from multisatellite observations for hydrological and climate studies. Bull Am Meteorol Soc 96(1):69–83. https://doi.org/10.1175/BAMS-D-13-00068.1

Bagley JE, Desai AR, Harding KJ, Snyder PK, Foley JA (2014) Drought and deforestation: has land cover change influenced recent precipitation extremes in the Amazon? J Clim 27(1):345–361. https://doi.org/10.1175/JCLI-D-12-00369.1

Barichivich J, Gloor E, Peylin P, Brienen RJW, Schöngart J, Espinoza JC, Pattnayak KC (2018) Recent intensification of Amazon flooding extremes driven by strengthened Walker circulation. Sci Adv 4(9): eaat8785. https://doi.org/10.1126/sciadv.aat8785

Carvalho LMV, Jones C, Liebmann B, Carvalho LMV, Jones C, Liebmann B (2004) The South Atlantic convergence zone: intensity, form, persistence, and relationships with intraseasonal to interannual activity and extreme rainfall. J Clim 17(1):88–108. https://doi.org/10.1175/1520-0442(2004)017<0088:TSACZI>2.0.CO;2

Coe MT, Costa MH, Botta A, Birkett C (2002) Long-term simulations of discharge and floods in the Amazon basin. J Geophys Res 107(D20):8044. https://doi.org/10.1029/2001JD000740

Coe MT, Costa MH, Soares Filho BS (2009) The influence of historical and potential future deforestation on the stream flow of the Amazon River - land surface processes and atmospheric feedbacks. J Hydrol (Amsterdam) 369(1/2):165–174. https://doi.org/10.1016/j.jhydrol.2009.02.043

Coelho C, Cavalcanti I, Ito R, Luz G, Santos L, Nobre CA, Marengo JA, Pezza AB (2013) As secas de 1998, 2005 e 2010. Analise climatologica. In: De Simone Borma L, Nobre CA (eds) Secas na Amazonia: Causas e Consequencias. Oficina de Textos Press, Sao Paulo, pp 89–116

Costa MH, Pires GF (2010) Effects of Amazon and Central Brazil deforestation scenarios on the duration of the dry season in the arc of deforestation. Int J Climatol 30(13):1970–1979. https://doi.org/10.1002/joc.2048

Da Silva PE, Santos e Silva CM, Spyrides MHC, Andrade L d MB (2019) Precipitation and air temperature extremes in the Amazon and Northeast Brazil. Int J Climatol 39(2):579–595. https://doi.org/10.1002/joc.5829

Davidson EA, De Araüjo AC, Artaxo P, Balch JK, Brown IF, Mercedes MM et al (2012) The Amazon basin in transition. Nature 481(7381): 321–328. https://doi.org/10.1038/nature10717

Debortoli NS, Dubreuil V, Funatsu B, Delahaye F, Henke De Oliveira C, Rodrigues-Filho S et al (2015) Rainfall patterns in the southern Amazon: a chronological perspective (1971-2010). Clim Chang 132:251–264. https://doi.org/10.1007/s10584-015-1415-1

Donat MG, Lowry AL, Alexander LV, O'Gorman PA, Maher N (2016) More extreme precipitation in the world's dry and wet regions. Nat Clim Chang 6(5):508–513. https://doi.org/10.1038/nclimate2941

ElNesr MN, Abu-Zreig MM, Alazba AA, ElNesr MN, Abu-Zreig MM, Alazba AA (2010) Temperature trends and distribution in the Arabian peninsula. Am J Environ Sci 6(2):191–203. https://doi.org/10.3844/ajessp.2010.191.203

Eltahir EAB, Bras RL (1994) Precipitation recycling in the Amazon basin. Q J R Meteorol Soc 120(518):861–880. https://doi.org/10.1002/qj.49712051806

Espinoza JC, Chavez S, Ronchail J, Junquas C, Takahashi K, Lavado W (2015) Rainfall hotspots over the southern tropical Andes: spatial distribution, rainfall intensity, and relations with large-scale atmospheric circulation. Water Resour Res 51(5):3459–3475. https://doi.org/10.1002/2014WR016273

Espinoza JC, Ronchail J, Marengo JA, Segura H (2019) Contrasting north–south changes in Amazon wet-day and dry-day frequency and related atmospheric features (1981–2017). Clim Dyn 52(9–10):5413–5430. https://doi.org/10.1007/s00382-018-4462-2

Fearnside PM (2000) Global warming and tropical land-use change: greenhouse gas emissions from biomass burning, decomposition and soils in forest conversion, shifting cultivation and secondary vegetation. Clim Chang 46(1/2):115–158. https://doi.org/10.1023/A:1005569915357

Fearnside PM (2015) Deforestation soars in the Amazon. Nature 521(7553):423–423. https://doi.org/10.1038/521423b

Freitas ACV, Ambrizzi T (2015) Recent changes in the annual mean regional Hadley circulation and their impacts on South America. Adv Meteorol 2015. https://doi.org/10.1155/2015/780205

Fryzlewicz P (2014) Wild binary segmentation for multiple change-point detection. Ann Stat 42(6):2243–2281. https://doi.org/10.1214/14-AOS1245

Fu R, Dickinson RE, Chen M, Wang H, Fu R, Dickinson RE, … Wang H (2001). How do tropical sea surface temperatures influence the seasonal distribution of precipitation in the equatorial Amazon? J Clim, 14(20), 4003–4026. https://doi.org/10.1175/1520-0442(2001)014<4003:HDTSST>2.0.CO;2

Fu G, Charles SP, Kirshner S (2013) Daily rainfall projections from general circulation models with a downscaling nonhomogeneous hidden Markov model (NHMM) for south-eastern Australia. Hydrol Process 27(25):3663–3673. https://doi.org/10.1002/hyp.9483

Funatsu BM, Dubreuil V, Claud C, Arvor D, Gan MA (2012) Convective activity in Mato Grosso state (Brazil) from microwave satellite observations: comparisons between AMSU and TRMM data sets. J Geophys Res Atmos 117(16):1–16. https://doi.org/10.1029/2011JD017259

Funk C, Peterson P, Landsfeld M, Pedreros D, Verdin J, Shukla S, Husak G, Rowland J, Harrison L, Hoell A, Michaelsen J (2015) The climate hazards infrared precipitation with stations—a new environmental record for monitoring extremes. Sci Data 2:150066. https://doi.org/10.1038/sdata.2015.66

Gloor M, Brienen RJW, Galbraith D, Feldpausch TR, Schöngart J, Guyot J-L et al (2013) Intensification of the Amazon hydrological cycle over the last two decades. Geophys Res Lett 40(9):1729–1733. https://doi.org/10.1002/grl.50377

Gocic M, Trajkovic S (2013) Analysis of changes in meteorological variables using Mann-Kendall and Sen's slope estimator statistical tests in Serbia. Glob Planet Chang 100:172–182. https://doi.org/10.1016/j.gloplacha.2012.10.014

Grimm AM, Zilli MT (2009) Interannual variability and seasonal evolution of summer monsoon rainfall in South America. J Clim 22(9): 2257–2275. https://doi.org/10.1175/2008JCLI2345.1

Gutiérrez-Vélez VH, DeFries R, Pinedo-Vásquez M, Uriarte M, Padoch C, Baethgen W et al (2011) High-yield oil palm expansion spares land at the expense of forests in the Peruvian Amazon. Environ Res Lett 6(4):044029. https://doi.org/10.1088/1748-9326/6/4/044029

Haylock MR, Peterson TC, Alves LM, Ambrizzi T, Anunciação YMT, Baez J et al (2006) Trends in Total and extreme south American rainfall in 1960–2000 and links with sea surface temperature. J Clim 19(8):1490–1512. https://doi.org/10.1175/JCLI3695.1

Huffman GJ, Bolvin DT, Nelkin EJ, Wolff DB, Adler RF, Gu G et al (2007) The TRMM multisatellite precipitation analysis (TMPA): quasi-global, multiyear, combined-sensor precipitation estimates at fine scales. J Hydrometeorol 8(1):38–55. https://doi.org/10.1175/JHM560.1

Instituto Nacional de Pesquisas Espaciais and National Institute for Space Research Projeto Prodes Monitoramento da Florsta Amazonica Brasileira por Sate'lite Prodes (2011) Retrieved April 16, 2019, from http://www.obt.inpe.br/OBT/assuntos/programas/amazonia/prodes. Accessed 16 April 2019

Kendall MG (1995) Rank Correlation Methods. Charles Griffin and Company: London. Second Edition

Khanna J, Medvigy D, Fueglistaler S, Walko R (2017) Regional dry-season climate changes due to three decades of Amazonian

deforestation. Nat Clim Chang 7(3):200–204. https://doi.org/10.1038/nclimate3226

Kleeman R (1989) A modeling study of the effect of the Andes on the summertime circulation of tropical south America. J Atmos Sci 46:3344–3362

Kumar Sen P (1968) Estimates of the regression coefficient based on Kendall's Tau. J Am Stat Assoc 63(324):1379–1389

Lau WKM, Kim K-M (2015) Robust Hadley circulation changes and increasing global dryness due to CO 2 warming from CMIP5 model projections. Proc Natl Acad Sci 112(12):201418682–201413635. https://doi.org/10.1073/pnas.1418682112

Laurance WF, Lovejoy TE, Vasconcelos HL, Bruna EM, Didham RK, Stouffer PC, … John Heinz H (2002) Ecosystem decay of Amazonian forest fragments: a 22-year investigation. Conserv Biol 16(3):605–618

Laurance WF, Camargo JLC, Fearnside PM, Lovejoy TE, Williamson GB, Mesquita RCG, Meyer CFJ, Bobrowiec PED, Laurance SGW (2018) An Amazonian rainforest and its fragments as a laboratory of global change. Biol Rev 93(1):223–247. https://doi.org/10.1111/brv.12343

Li W, Fu R (2004) Transition of the large-scale atmospheric and land surface conditions from the dry to the wet season over Amazonia as diagnosed by the ECMWF re-analysis. J Clim 17(13):2637–2651. https://doi.org/10.1175/1520-0442(2004)017<2637:TOTLAA>2.0.CO;2

Li W, Fu R, Dickinson RE (2006) Rainfall and its seasonality over the Amazon in the 21st century as assessed by the coupled models for the IPCC AR4. J Geophys Res Atmos 111(2):1–14. https://doi.org/10.1029/2005JD006355

Liebmann B, Marengo JA (2001) Interannual variability of the rainy season and rainfall in the Brazilian Amazon Basin. J Clim 14(22):4308–4318. https://doi.org/10.1175/1520-0442(2001)014<4308:IVOTRS>2.0.CO;2

Liebmann B, Kiladis GN, Vera CS, Saulo AC, Carvalho LMV (2004) Subseasonal variations of rainfall in South America in the vicinity of the low-level jet east of the Andes and comparison to those in the South Atlantic convergence zone. J Clim 17(19):3829–3842. https://doi.org/10.1175/1520-0442(2004)017<3829:SVORIS>2.0.CO;2

Longobardi P, Montenegro A, Beltrami H, Eby M (2016) Deforestation induced climate change: effects of spatial scale. PLoS One 11(4). https://doi.org/10.1371/journal.pone.0153357

Malhi Y, Wood D, Baker TR, Wright J, Phillips OL, Cochrane T et al (2006) The regional variation of aboveground live biomass in old-growth Amazonian forests. Glob Chang Biol 12(7):1107–1138. https://doi.org/10.1111/j.1365-2486.2006.01120.x

Mann HB (1945) Nonparametric tests against trend. Econometrica 13(3):245. https://doi.org/10.2307/1907187

Marengo JA (2004) Interdecadal variability and trends of rainfall across the Amazon basin. Theor Appl Climatol 78(1–3):79–96. https://doi.org/10.1007/s00704-004-0045-8

Marengo JA, Espinoza JC (2016) Extreme seasonal droughts and floods in Amazonia: causes, trends and impacts. Int J Climatol 36(3):1033–1050. https://doi.org/10.1002/joc.4420

Marengo JA, Nobre CA, Tomasella J, Oyama MD, Sampaio de Oliveira G, de Oliveira R et al (2008) The drought of Amazonia in 2005. J Clim 21(3):495–516. https://doi.org/10.1175/2007JCLI1600.1

Moore N, Arima E, Walker R, Ramos da Silva R (2007) Uncertainty and the changing hydroclimatology of the Amazon. Geophys Res Lett 34:14707. https://doi.org/10.1029/2007GL030157

Nepstad DC, Stickler CM, Soares-Filho B, Merry F (2008) Interactions among Amazon land use, forests and climate: prospects for a near-term forest tipping point. Philos Trans R Soc B Biol Sci 363(1498):1737–1746. https://doi.org/10.1098/rstb.2007.0036

Nobre CA, Sampaio G, Borma LS, Castilla-Rubio JC, Silva JS, Cardoso M (2016) Land-use and climate change risks in the Amazon and the need of a novel sustainable development paradigm. Proc Natl Acad Sci 113(39):10759–10768. https://doi.org/10.1073/pnas.1605516113

Oyama MD, Nobre CA (2003) A new climate-vegetation equilibrium state for Tropical South America. Geophys Res Lett 30(23), n/a-n/a). https://doi.org/10.1029/2003GL018600

Paccini L, Espinoza JC, Ronchail J, Segura H (2018) Intra-seasonal rainfall variability in the Amazon basin related to large-scale circulation patterns: a focus on western Amazon–Andes transition region. Int J Climatol 38(5):2386–2399. https://doi.org/10.1002/joc.5341

Partal T, Kahya E (2006) Trend analysis in Turkish precipitation data. Hydrol Process 20(9):2011–2026. https://doi.org/10.1002/hyp.5993

R Core Team (2018) R: a language and environment for statistical computing. R Foundation for Statistical Computing, Vienna, Austria Retrieved from http://www.r-project.org/. Accessed 24 May 2019

Rohrbeck C (2013) Detection of changes in variance using binary segmentation and optimal partitioning. Retrieved from https://www.semanticscholar.org/paper/Detection-of-changes-in-variance-using-binary-and-Rohrbeck/b132976b756634c02a8bdd77d4c530d02222561a. Accessed 17 June 2019

Ronchail J, Cochonneau G, Molinier M, Guyot JL, De Miranda Chaves AG, Guimarães V, De Oliveira E (2002) Interannual rainfall variability in the Amazon basin and sea-surface temperatures in the equatorial Pacific and the tropical Atlantic oceans. Int J Climatol 22(13):1663–1686. https://doi.org/10.1002/joc.815

Saad SI, da Rocha HR, Silva Dias MAF, Rosolem R, Saad SI, da Rocha HR et al (2010) Can the deforestation breeze change the rainfall in Amazonia? A case study for the BR-163 highway region. Earth Interact 14(18):1–25. https://doi.org/10.1175/2010EI351.1

Saatchi SS, Houghton RA, Dos Santos Alvalá RC, Soares JV, Yu Y (2007) Distribution of aboveground live biomass in the Amazon basin. Glob Chang Biol 13(4):816–837. https://doi.org/10.1111/j.1365-2486.2007.01323.x

Salviano MF, Daniel Groppo J, Pellegrino GQ (2016) Trends analysis of precipitation and temperature data in Brazil. Rev Brasil Meteorol 31(1):64–73. https://doi.org/10.1590/0102-778620150003

Santos EB, Lucio PS, Silva CMSE (2015) Precipitation regionalization of the Brazilian Amazon. Atmos Sci Lett 16(3):185–192. https://doi.org/10.1002/asl2.535

Satyamurty P, de Castro AA, Tota J, da Silva Gularte LE, Manzi AO (2010) Rainfall trends in the Brazilian Amazon Basin in the past eight decades. Theor Appl Climatol 99(1–2):139–148. https://doi.org/10.1007/s00704-009-0133-x

Sharma D, Babel MS (2014) Trends in extreme rainfall and temperature indices in the western Thailand. Int J Climatol 34(7):2393–2407. https://doi.org/10.1002/joc.3846

Sheil D, Murdiyarso D (2009) How forests attract rain: an examination of a new hypothesis. BioScience 59(4):341–347. https://doi.org/10.1525/bio.2009.59.4.12

Silva CHL Jr, Almeida CT, Santos JRN, Anderson LO, Aragão LEOC, Silva FB (2018) Spatiotemporal rainfall trends in the Brazilian legal Amazon between the years 1998 and 2015. Water (Switzerland) 10(9):1–16. https://doi.org/10.3390/w10091220

Sombroek W (2001) Spatial and temporal patterns of Amazon rainfall. AMBIO 30(7):388–396. https://doi.org/10.1579/0044-7447-30.7.388

Spera SA, Galford GL, Coe MT, Macedo MN, Mustard JF (2016) Land-use change affects water recycling in Brazil's last agricultural frontier. Glob Chang Biol 22(10):3405–3413. https://doi.org/10.1111/gcb.13298

Vera C, Silvestri G, Liebmann B, González P (2006) Climate change scenarios for seasonal precipitation in South America from IPCC-AR4 models. Geophys Res Lett 33:13707. https://doi.org/10.1029/2006GL025759

Walker R, Moore NJ, Arima E, Perz S, Simmons C, Caldas M, Vergara D, Bohrer, C (2009) Protecting the Amazon with protected areas. Proceedings of the National Academy of Sciences of the United

States of America 106(26):10582–10586. https://doi.org/10.1073/pnas.0806059106

Wilks DS (2011) Statistical methods in the atmospheric sciences. Elsevier/Academic Press, 3rd Edition

Wright JS, Fu R, Worden JR, Chakraborty S, Clinton NE, Risi C, Sun Y, Yin L (2017) Rainforest-initiated wet season onset over the southern Amazon. Proc Natl Acad Sci U S A 114(32):8481–8486. https://doi.org/10.1073/pnas.1621516114

Wu M, Schurgers G, Ahlström A, Rummukainen M, Miller PA, Smith B, May W (2017) Impacts of land use on climate and ecosystem productivity over the Amazon and the South American continent. Environ Res Lett 12(5):054016. https://doi.org/10.1088/1748-9326/aa6fd6

Xu, Z. X., Takeuchi K, Ishidaira H (2003) Monotonic trend and step changes in Japanese precipitation. J Hydrol, 279(1–4), 144–150. https://doi.org/10.1016/S0022-1694(03)00178-1

Yin L, Fu R, Zhang Y-F, Arias PA, Fernando DN, Li W, … Bowerman AR (2014) What controls the interannual variation of the wet season onsets over the Amazon? Journal of Geophysical Research: Atmospheres, 119(5), 2314–2328. https://doi.org/10.1002/2013JD021349

Yoon JH, Zeng N (2010) An Atlantic influence on Amazon rainfall. Clim Dyn 34(2):249–264. https://doi.org/10.1007/s00382-009-0551-6

Zilli MT, Carvalho LMV, Liebmann B, Silva Dias MA (2017) A comprehensive analysis of trends in extreme precipitation over southeastern coast of Brazil. Int J Climatol 37(5):2269–2279. https://doi.org/10.1002/joc.4840